COBEM 2023 27TH INTERNATIONAL CONGRESS OF MECHANICAL ENGENEERING

ABCM Brazilian Society of Mechanical Sciences and Engineering
27th ABCM International Congress of Mechanical Engineering
December 04-08, 2023, Florianópolis-SC, Brazil

COB2023-1614

# 3D Finite Elements Analysis through Beam-to-Beam Contacts on Transmission Line Conductors

**Bruno Jardim Pedrosa**
**José Alexander Araújo**
**Jorge Luiz de Almeida Ferreira**
**Remy Kalombo Badibanga**
**Luís Augusto Conte Mendes Veloso**
Universidade de Brasília, Campus Universitário Darcy Ribeiro 70910-900, Asa Norte, Brasília-DF
bruno.pedrosa10@gmail.com

***Abstract.*** *This work presents a parametric numerical model, with low computational cost, based on Finite Element Method for the analysis of multilayer wire conductors subjected to tensile and bending loads. For such, routines are implemented on the software ANSYS/APDL that allow parameterization of mechanical and geometric characteristics of metallic wire conductors. Such capacity enables the analysis of diverse configurations of cables and simulations. The wire elements are discretized through beam elements BEAM 198 and the interwire contacts are established through elements TARGE 170 (master) CONTA 177 (slave). The parametric numerical model is applied in tensile and tension-bending simulations, being compared with analytical results and numerical results present in the literature. The simulations show good results compared to numerical and analytical models. The tensile simulations presented average percentage differences in axial stress of 3,5% compared to analytical results and 11% compared to numerical results from the literature. The axial displacement, due to traction, also shows proximity to analytical results with an average percentage difference of 7%. The tensile-bending simulations demonstrate behavior consistent with analytical values, the deflection curve along the axial axis is between the maximum and minimum analytical values, as expected. These results attest to the validation of the current numerical model.*

***Keywords:*** *Multilayered wire conductor, Overhead conductor, Finite element method, ANSYS APDL, Beam Element, Beam-to-beam contact.*

## 1. INTRODUCTION

Finite Elements $(FE)$ simulations of multilayered metal cables have been a challenge studied for decades and traditionally the models are based on 3D solid element discretization of every wire in the cable. Such method implies heavy $FE$ models with a high number of elements, degrees of freedom and, most importantly, high computational cost (Stanová *et al.*, 2011).

In order to correctly analyse mechanical strain and bending in multilayered metal cables, contact between individual wires must be correctly simulated, this implies multiple contact points, which, in turn, guarantee non linear regime and high computational cost, as seen in Stanová *et al.* (2011) whose simulations had an average time of 21 hours.

The theory proposed by Papailiou (1997) for cables under traction and bending stresses hypothesises that the magnitude of tensions in wires depends on the frictional contact between the individual wires. In this situation, the bending stiffness of the conductor is a function of the friction and contact forces on each wire. This bending stiffness varies from a minimum, where it is assumed that two wires in the section slide with no friction against each other, to a maximum where there is no sliding between the wires.

Given the theory of Papailiou (1997), following researchers further developed the field. In regard to computational methods, Nawrocki and Labrosse (2000), MA *et al.* (2008), Stanová *et al.* (2011) and Judge *et al.* (2012) demonstrate through $FE$ simulations different cables with different materials, all with good convergence of experimental and analytical data, yet these models all utilize 3D solid elements with over $150.000$ elements and computational times in the range of several hours to a day.

Recently, in focus of reducing computational costs of simulations, Lalonde *et al.* (2017) shows a model based on beam elements aided by contact elements for discretization of wires and their contact. This approach leads to a drastic decrease in the number of elements and degrees of freedom, resulting in computational costs up to two orders of magnitude lower. The simulation results of Lalonde *et al.* (2017) are compared to experimental data and to the numerical results of Judge *et al.* (2012), proving the methodology with 2640 beam elements, 5869 contact pairs and 62 minutes of processing time. Judge *et al.*'s $FE$ simulation, in contrast, takes 12 hours of processing time with $2.520.000$ elements for the same problem.

The present paper validates a numerical parametric finite element model for multilayer conductor cables with low

computational cost, based on the study of Lalonde *et al.* (2017), built and simulated in ANSYS/APDL. In order to validate such model, two simulations are presented: An axial force on a $1X37$ conductor compared with results obtained by Wu (2014) and by analytical calculations of the cable's resultant elongation; An axial and bending forces on a $1X7$ cable compared with the maximum and minimum analytical lines of bending stiffness as demonstrated by Papailiou (1997).

## 2. MODELING

### 2.1 General Geometry of Conductors

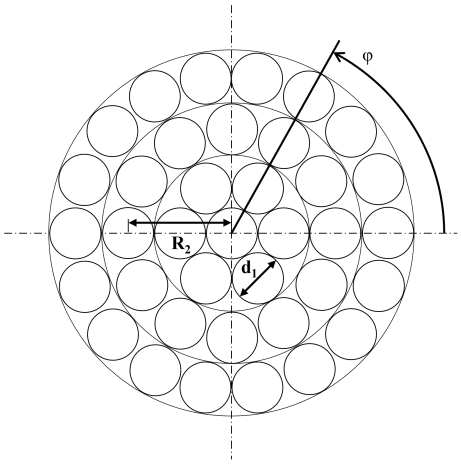


Figure 1. Cross-sectional view of a conductor with three layers and examples of average radii.

Multilayered metal cables are composed of wires wound around a center wire forming layers that are added upon the previous one, creating the geometry shown in Fig. 1. These cables are made in Planetary Stranding Machines that feed a core wire at its center, while the wires of the layers are introduced peripherally towards the core wire by a rotating head feeder. In this way, the core remains straight while the wires of a specific layer are braided around the core with the same pitch, angle, and spacing between them, thus producing the characteristic helical geometry of a conductor cable.

This wrapping of each layer occurs in accordance with the lay angle $\beta$ in respect to the center axis. Usually, adjacent layers have opposing lay angles, and the following examples in this paper all follow this case.

The third main variable of layered metal conductors is the helical angle $\phi$, as shown in Fig. 1. Which describes the position angle of each wire's cross-section relative to the axial axis of the cable. As the cable follows its path, the angle $\phi$ will vary from 0 to $2\pi$ until it reaches the end of the rotation.

Figure 1 also presents the average radii of each layer $R(k)$ along with each layer's wire diameter $d_k$. Given these values, it is possible to create equations that describe the helical trajectory of each wire $j$ in each layer $k$:

$$X(k,j) = R(k)cos\phi(j), \tag{1}$$

$$Y(k,j) = R(k)sen\phi(j), \tag{2}$$

$$Z(k,j) = \frac{R(k)\phi(j)}{tan\beta(k)}, \tag{3}$$

### 2.2 ANSYS Geometry Modeling

Implementing any geometry in ANSYS/APDL starts with creating the Keypoints, and from them, the lines or volumes that represent the problem's geometry. In the present paper, the $FE$ model approach only requires keypoints proceeded by lines that represent the helical path of the wire's center lines around the layers as described by Lalonde *et al.* (2017). Each Keypoint needs its $X$, $Y$ and $Z$ coordinates to be generated, so the following equations describe the helical path of each wire.

$$X(i,j,k) = R(k)cos\left(\frac{2\pi(i-1)}{(L-1)}\frac{(h_{ext})}{(h(k))} + \phi_0(j)\right), \tag{4}$$

$$Y(i,j,k) = R(k)sen\left(\frac{2\pi(i-1)}{(L-1)}\frac{(h_{ext})}{(h(k))} + \phi_0(j)\right), \tag{5}$$

$$Z(i,j,k) = \frac{R(k)\left(\frac{2\pi(i-1)}{(L-1)}\frac{(h_{ext})}{(h(k))}\right)}{tan(\beta(k))}, \tag{6}$$

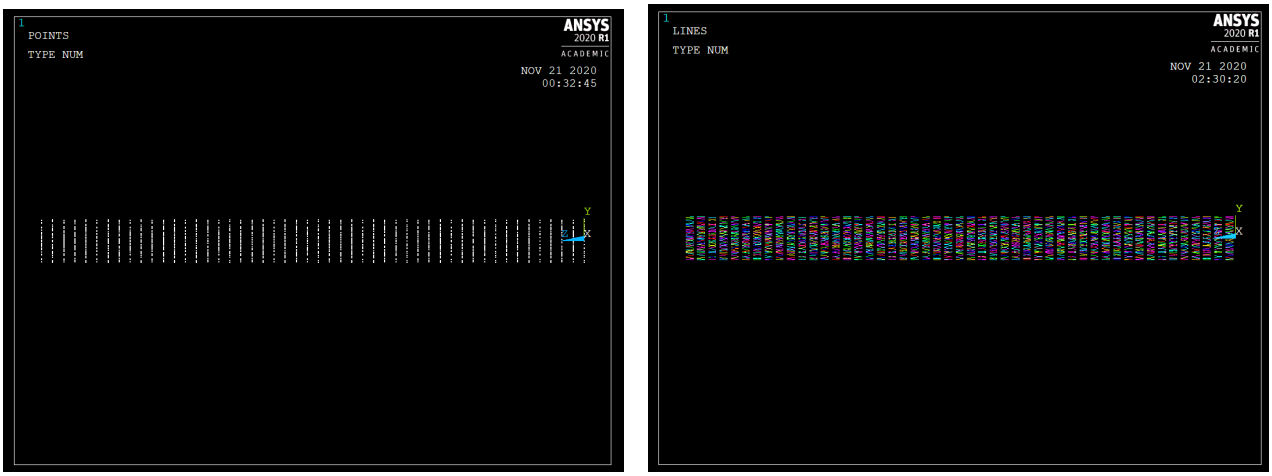


Figure 2. Side view of a 3 layer $1X37$ conductor. (A): *keypoints*; (B): Lines.

where $i$ from 1 to $L$ discreet keypoints in the wire's path, $j$ from 1 to $n$ wires of a particular layer $k$, $\phi_0(j)$ is the phase angle, $h_{ext}$ and $h(k)$ are the layer rotation step compatibility equations for the most external ($h_{ext}$) layer in the model and the layer currently being created ($h_k$).

The phase angle $\phi_0(j)$ is a counter, it is necessary to create the other wires of a layer, it adds the starting angle position $\phi_0$ to $\phi$ in a manner to offset the starting keypoint of wires in a layer and avoid overlay of their cross section.

$$\phi_0(j) = \frac{2\pi(j-1)}{n} \tag{7}$$

The terms $h_{ext}$ and $h(k)$ in Eq. 4, 5 and 6, guarantee that every wire will be sectioned with the same number of elements and most importantly, all elements will have the same horizontal length, Fig. 2a. This aids by discretizing the models future mesh, which is dependent only on the lines between Keypoints, shown in Fig. 2b, and avoiding problems in interpolation of contact points.

$$h(k) = \frac{2\pi R(k)}{tan(\beta(k))} \tag{8}$$

Therefore, by applying both concepts of starting phase angle $\phi_0$ and layer rotation step compatibility $h(k)$ into the helical angle. For each Keypoint along the any wire's path, $\phi$ assumes the following format:

$$\phi(i,k) = 2\pi\frac{(i-1)}{(L-1)}\frac{(h_{ext})}{(h(k))} + \phi_0(j). \tag{9}$$

### 2.3 Properties of the Conductors

Two different conductor models are chosen from two different sources, Wu (2014) and Papailiou (1995), with the goal to verify if the present model does indeed give similar results to proven examples in diverse literature.

#### 2.3.1 Three Layer Conductor for Traction Simulations

The studied $1X37$ wires conductor for the traction simulations is compared to the work of Wu (2014) and its parameters are presented in Tab. 1.

Table 1. Properties of the $(1X37)$ Conductor.
Total Length: $L$=100 $mm$.

| **Layer** | **N° of Wires** | **Wire diameter** | **Layer Radii** $R(k)$ | **Lay angle** $\beta$ |
|---|---|---|---|---|
| Core | 1 | $1,35\ mm$ | - | $0°$ |
| 1 | 6 | $1,25\ mm$ | $1,3\ mm$ | $14°$ |
| 2 | 12 | $1,25\ mm$ | $2,55\ mm$ | $14°$ |
| 3 | 18 | $1,25\ mm$ | $3,8\ mm$ | $14°$ |

The material Young's Modulus is $E = 188\ GPa$ and, as all wires are aluminium, it's density is $q = 7.800 kg/m^3$, Poisson's ratio is $\upsilon = 0,3$ and the Friction Coefficient is $\mu = 0,2$. All in accordance to the model of Wu (2014).

### 2.3.2 One Layer Conductor for Bending Simulation

The aluminium/steel $1X7$ wires ACSR DIN 48204 conductor utilized by Papailiou (1995) for bending simulations is also present in this work, it's parameters are presented in Tab. 2. This cable would usually have more layers, but the student version of ANSYS/APDL can not support the number of nodes required to model it, and Papailiou (1995) also only considers the core and first layer in its work.

Table 2. Properties of the $(1X7)$ Conductor.
Total Length: $L$=1000 $mm$.

| **Layer** | **N° of Wires** | **Wire diameter** | **Layer Radii** $R(k)$ | **Lay angle** $\beta$ |
|---|---|---|---|---|
| Core | 1 | $2,7\ mm$ | - | $0°$ |
| 1 | 6 | $2,7\ mm$ | $2,7\ mm$ | $10°$ |

As stated by Papailiou (1995), the material Young's Modulus is $E = 210\ GPa$ for the steel core wire and $E = 70\ GPa$ for the aluminium wires in the first and only layer. Poisson's ratio is $\upsilon = 0,3$. In order to verify if the current model responds correctly to variations in its parameters, there are three simulations, each with one Friction Coefficient of $0,1$ , $0,3$ and $0,5$.

## 3. FE Model and Problem Generation

ANSYS/APDL supports its own language for inputting commands, so the geometric model and its defining equations are written in a .txt file and later inputted into ANSYS/APDL.

The 1X7 conductor mesh has $4.193$ nodes, $2.093$ BEAM 189 beam elements, and $5.681$ TARGE 170/CONTA 177 contact elements. The final mesh of the 1X37 conductor has $3.663$ nodes, $18.865$ TARGE 170/CONTA 177 contact elements, and $1.813$ BEAM 189 beam elements.

The machine used in this work features an Intel i5-11600K processor with 6 cores @ $3,90\ GHz$, 16 $GB$ of DDR4 RAM, and an NVIDIA GeForce GTX 1060 graphics card with 6 $GB$ of DDR4 memory.

### 3.1 Beam Elements

Following the work of Lalonde *et al.* (2017), the center line of each wire has been created in the previous steps and is essentially defined by $L$ lines (see Equations 4, 5 and 6) describing the helical path. Lalonde *et al.* (2017) uses each one of these lines as the basis for the BEAM 189 element.

The BEAM189 element is a 3D three node elements suitable for slender beam structures and supports elastic and plastic deformations (ANSYS APDL User's Guide, 2022), both required when studying multilayered conductors. This method represents the wire as various smaller beams connected back-to-back.

On the topic of mesh refinement, in the $FE$ approach of Lalonde *et al.* (2017), given that each element is a small straight beam section (BEAM189 element), the increase in $L$ lines chosen for the geometry model entails in each wire having more partitions, more nodes and it being more refined. Lalonde *et al.* (2017) compares this method to full 3D cubic elements $FE$ simulations, as well as physical experiments and shows that elements with up to $10\ mm$ in length are appropriate for traction and bending analysis of conductors.

With this as guidance, the present paper chooses elements with $2\ mm$ of length for the $100\ mm$ 3-layer cable under traction, which translates to $L = 50$ line partitions. For the 1-Layer $1000\ mm$ conductor, there are $L = 300$ line partitions presenting elements with $3,33\ mm$ of length.

### 3.2 Contact Elements

For the contact interactions, Lalonde *et al.* (2017) proposes the CONTA177 and the TARGE170 elements to create a pair-based contact model. These elements are also recommended by the ANSYS APDL User's Guide (2022) for the case of 3D beam-to-beam surfaces in contact, either sticking or sliding. The CONTA177 element also has the option for optimizing for crossing or parallel beam contacts, as seem in Fig. 3.

Each pair of elements assumes the status, in ANSYS/APDL the function for such is "Real Constants", of crossing or parallel contact. All elements in a single wire (CONTA177) are paired to all wires on the layer above as crossing contact and paired as parallel contact with the next adjacent wires in it's layer. In this manner, every possible interaction for a element is covered and the model is ready for implementation in simulations.

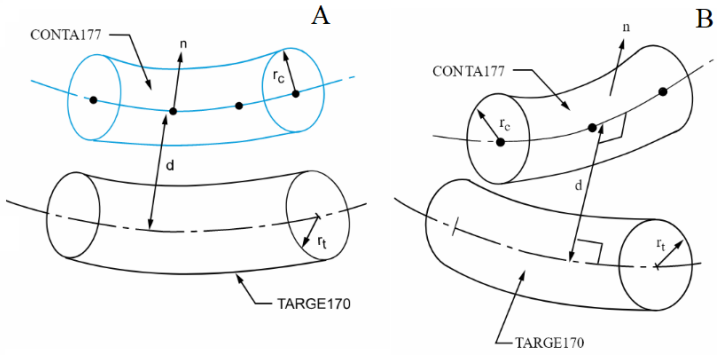


Figure 3. Element CONTA177 options for parallel (A) or crossing (B) beams in contact.
(ANSYS APDL User's Guide, 2022)

### 3.3 Simulations

#### 3.3.1 3-Layer Conductor under Traction

The present simulation aims to replicate a small span in the middle of a conductor under traction, with no interference of support equipment, such as clamps or any restricting apparatus.

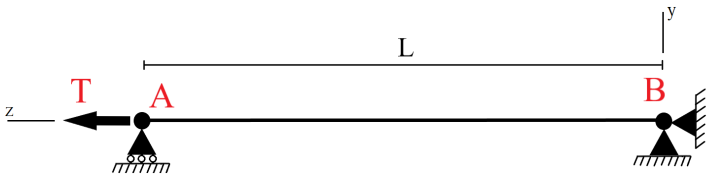


Figure 4. Conductor under traction and boundary conditions

Figure 4 shows the diagram of the traction simulation for the three layer cable of Wu (2014)'s work. It is a simple traction simulation with one end of the conductor with movement restrictions, $u_x = u_y = u_z = 0$, and the other end has a support that allows only axial movement $u_z$. The points are, respectively, $B$ and $A$ in Fig. 4.

No bending moment restriction is applied, this is due to the observations of Nawrocki and Labrosse (2000), where there are wires that roll and pivot amongst themselves, making it impossible to apply restrictive conditions of bending moments on a surface that simulates the possible middle of a conductor's span.

$A$ and $B$ in Fig. 4 are the end surfaces of the conductor, in the present work, both the boundary conditions and force $T$ are applied/distributed on all nodes of the surface (i.e. these nodes are the most extreme node of each wire).

Following the work of Wu (2014), four simulations are made, each with it's load: $T_1 = 13.600N$, $T_2 = 20.000N$, $T_3 = 25.000N$ and $T_4 = 30.000N$. The load is distributed equally throughout the surface $A$ by the coupling of the nodes, meaning that all nodes will have to displace equally with the applied load.

For comparison, the analytical formulation of Cardou (2013) and the full 3D $FE$ model of Wu (2014) are used and the average tensions in each layer is evaluated.

#### 3.3.2 1-Layer Conductor under Bending

This simulation aims to replicate the experiments of Papailiou (1995), where a meter long 1-layer conductor receives, simultaneously, an axial traction force, $T = 2.000N$, and a vertical bending force on it's halfway mark, $V = 500N$.

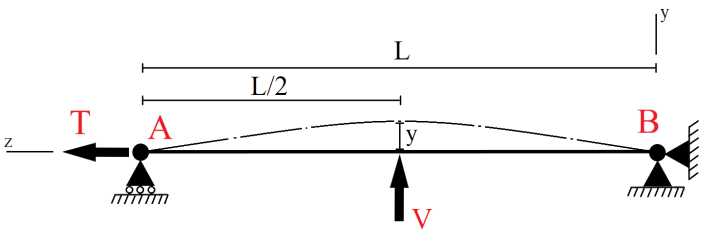


Figure 5. Conductor under bending and boundary conditions

For the bending simulation of the 1 layer conductor, the present method applies two steps, first the traction $T = 2.000N$ is fully loaded and the pure traction simulation is run. Then, as a second load step, all nodes in $A$ (see. Fig.5) are

restricted, $u_x = u_y = u_z = 0$, and finally, the vertical force $V = 500N$ is loaded in the center node of the core wire. The node restriction guarantees that the tensioned position will be held in place and the force $V$ will not pull the $A$ surface back.

This is done in accordance to Lalonde *et al.* (2017) that performs a similar simulation, stipulates this methodology and shows good results. For that matter, unlike this paper's previous simulation, the bending moments are all restricted on points $A$ and $B$, $M_{xy} = M_{xz} = M_{yz} = 0$, in order to follow the literature for the second and final load step.

The analytical data for comparison is summarized by the maximum ($EJ_{max}$) and minimum ($EJ_{min}$) bending stiffness of the theory of Papailiou (1997) for helical multilayered wires under bending. With these values, it is possible to verify whether the numerical displacement deflections in the $Y$ axis corresponds to the theoretical range of maximum and minimum. These deflection lines are given by Equation 10 presented in the work of Lalonde *et al.* (2017).

$$y(x) = \frac{VK}{2T}\left[\left(\sinh\left(\frac{x}{K}\right) - \frac{x}{K}\right) - \tanh\left(\frac{s}{K}\right)\left(\cosh\left(\frac{x}{K}\right) - 1\right)\right], \tag{10}$$

where $V = 500N$ and $T = 2.000N$, as previously stated, $x$ corresponds to the distance to the origin of the numerical model, and the variable $K$ is given by Lalonde *et al.* (2017) as:

$$K = \left(\frac{EJ}{T}\right)^{\frac{1}{2}}, \tag{11}$$

where $EJ$ is the bending stiffness based in the theory of Papailiou (1997), and varies between its maximum (Eq. 14) and minimum (Eq. 12), $J$ is the moment of inertia of the corresponding wire.

The minimum bending stiffness is defined by Papailiou (1997) as,

$$EJ_{min} = \sum_{1}^{n} EJ_w \cos\beta + EJ_c, \tag{12}$$

where $n$ is the sum of wires in all layers, $J_w$ and $J_c$ are the, corresponding, moments of inertia for the layer and core wires. $E$ is the Young's Modulus of the given wire.

To achieve the variation to maximum stiffness, a complementary bending stiffness (Eq.13) is added, this represents the additional resistance from the helical geometry of the layers above the center wire as explained by Papailiou (1997).

$$EJ_{compl} = 3A_w E_w R^2 \cos^2\beta, \tag{13}$$

where $A_w$ is the cross-sectional area of the wire, $R$ is the average radii of each layer and $\beta$ is the lay angle. By adding this term to the minimum, Eq.14 is reached and the analytical formulation for comparison to the numerical model is done.

$$EJ_{max} = EJ_{min} + EJ_{compl} \tag{14}$$

## 4. RESULTS AND DISCUSSIONS

### 4.1 Computational Cost

Achieving low computational is one of the main goals of the present work, Tab.3 shows three traction simulations, two of them found in the literature. The analysis of Stanová *et al.* (2011) is the very same as the one performed in this work with the exception of full 3D hexahedral elements that elevates drastically the computational cost, as seen in the total solution time in Tab.3.

Table 3. Traction simulations computational time for the present model and Stanová *et al.* (2011)

| **Present numerical model** | **Stanová et al. (2011)** |
|---|---|
| 37 wires | 37 wires |
| $T = 30kN$ | $T = 30kN$ |
| 1.813 beam elements | 152.347 full 3D elements |
| $2\ min$ | $1.260\ min$ |

### 4.2 3-Layer Conductor under Traction

The simulation results were compared with numerical results from Wu (2014) and with the analytical methodology of Papailiou (1997). The average normal tension comparisons for each layer are presented in Tab.4, which shows the

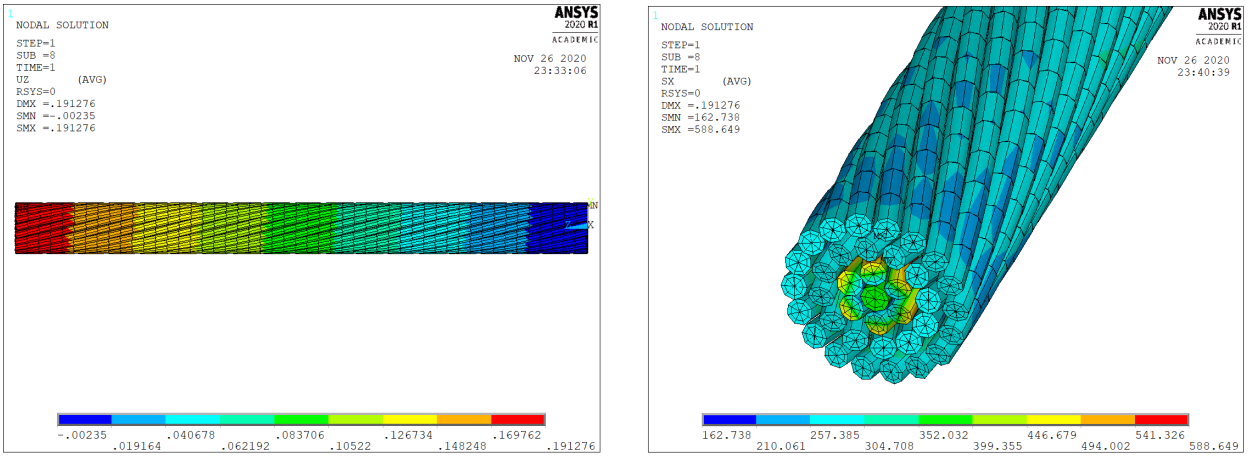


Figure 6. Results for the $F$= 13.680 $N$ of a 3 layer $1X37$ conductor. (A): Displacement $mm$; (B): Isometric view of Surface $A$'s normal tension $MPa$.

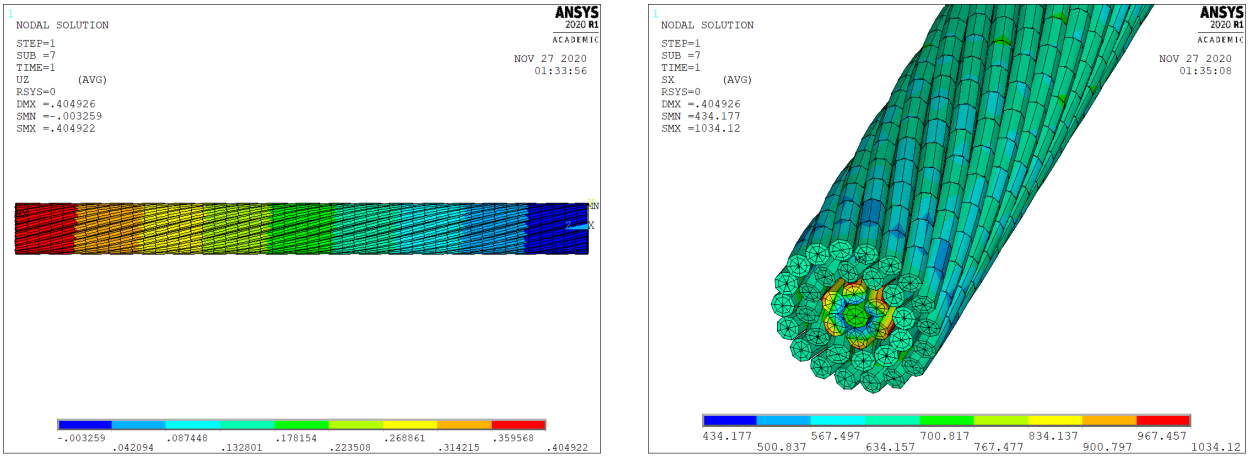


Figure 7. Results for the $F$= 30.000 $N$ of a 3 layer $1X37$ conductor. (A): Displacement $mm$; (B): Isometric view of Surface $A$, normal tension $MPa$ results.

average normal tension of the average of all wires for each layer, and two examples are presented in Fig.6.b and Fig.7.b. The results show a maximum percentage difference of $32\%$ compared to those obtained by Wu (2014). Additionally, the largest divergences are found in the core and the first layer. The same applies to the comparison with the analytical results, where the maximum percentage difference is $21\%$ and occurs in the same case and in the layer with the highest numerical discrepancy.

The specific normal stresses for each simulation are close to the analytical results. Furthermore, given the load variation in each case, the cable conductor $1X37$ behaves as expected. No cases with extremely discrepant normal stresses were observed, which could indicate an error in the generation of the numerical model. However, the exceptionally high stresses for the 1st layer must be emphasized as a reviewing point in further works, as it seems to be supporting a higher load than expected.

Figure 8 shows numerical and analytical values are obtained for the cable displacement ($\delta$) for each case (e.g. Fig. 6.a and Fig. 7.a). The behavior of the numerical model is as expected, given the similarity to the analytical line. However, in all cases, the displacement is on average $23\%$ lower than that presented by the simulation of Wu (2014). The literature indicates that for case 4, the total displacement should be approximately $0,5$ mm (Papailiou, 1997) and the model stands with a $20\%$ difference to it.

Differences like these are expected for a nonlinear simulation, especially when compared to analytical results that make assumptions and approximations. For example, the methodology of Cardou (2013) and Papailiou (1997), where it is possible to determine the equations for axial displacement and average normal stress without considering the friction coefficient of the material.

By observing the surface A, Fig. 6.a and Fig. 7.a, a high stress gradient between layer 1 and layer 2 can be noticed. This may show a load increase in the core and 1st layer that requires further testing. As demonstrated by Papailiou

Table 4. Average normal tension compared to analytical data and simulations of Wu (2014).

**Average Normal Tension (MPa)**

| Force (N) | Core | Wu (2014) Diff. % | Analytical Diff. % | 1st Layer | Wu (2014) Diff. % | Analytical Diff. % |
|---|---|---|---|---|---|---|
| 13.680 | 361,00 | **19%** | **11%** | 372,02 | **32%** | **21%** |
| 20.000 | 523,40 | **7%** | **9%** | 517,81 | **14%** | **15%** |
| 25.000 | 643,88 | **16%** | **8%** | 629,44 | **22%** | **12%** |
| 30.000 | 765,20 | **15%** | **7%** | 740,28 | **20%** | **10%** |
| **Average** | 573,37 | **14%** | **8%** | 564,89 | **21%** | **13%** |

| Force (N) | 2nd Layer | Wu (2014) Diff. % | Analytical Diff. % | 3rd Layer | Wu (2014) Diff. % | Analytical Diff. % |
|---|---|---|---|---|---|---|
| 13.680 | 290,49 | **0%** | **-5%** | 292,30 | **2%** | **-5%** |
| 20.000 | 432,74 | **2%** | **-4%** | 436,36 | **-2%** | **-3%** |
| 25.000 | 545,26 | **6%** | **-3%** | 549,13 | **5%** | **-3%** |
| 30.000 | 657,72 | **7%** | **-3%** | 662,12 | **9%** | **-2%** |
| **Average** | 481,55 | **5%** | **-4%** | 484,98 | **4%** | **-3%** |

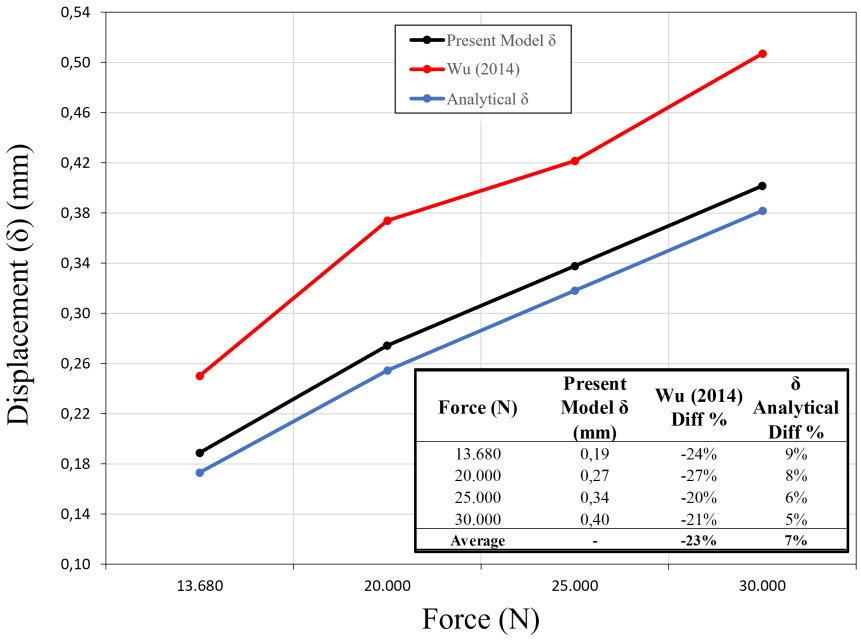


Figure 8. Axial displacement for a $1X37$ cable in the four cases.

(1997), lower layers do have higher average normal tensions since they support the layers above from collapsing inwards, but the present model does show an increase higher than the expected friction contact addition to the system. The higher tension may explain the negative $20\%$ difference of displacement ($\delta$), as the cable's model has a higher axial rigidity that further testing is required to fully comprehend. Apart from this, the average stress remains constant along the wires for all cases, indicating a good distribution of contact interactions along all wires. The same situation repeats for face B of the conductor.

### 4.3 1-Layer Conductor under Bending

For the bending simulations, the computational and analytical data were compared using the deflection line as a function of the position along the axis ($Y(x)$), commonly used in the works of Papailiou (1997) and Lalonde *et al.* (2017) to evaluate the behavior of numerical models.

Figure 10 presents the deflections in $Y(x)$ for the three simulations, and as expected, they follow the theoretical deflection for bending stiffness. The three friction coefficient conditions show dispersion in the final deflection, as reported in the literature, but there is an important point to note.

The works of Papailiou (1997) and Cardou (2013) state that numerical and experimental results should fall within the

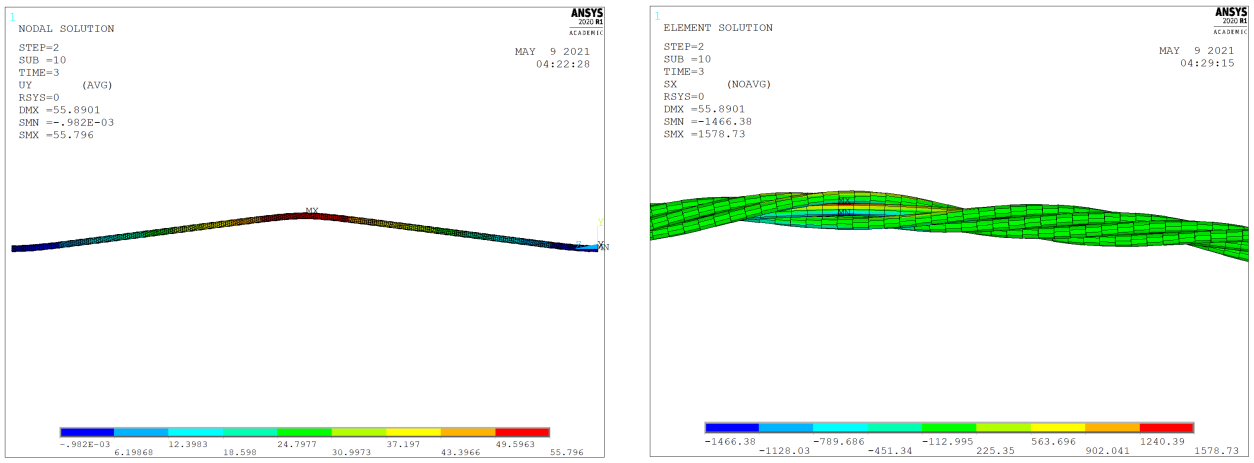


Figure 9. Lateral view of displacement (mm) and normal stress (MPa) results, $\mu$ = 0,3. (A) Displacement; (B) Normal Stress, zoomed in the halfway point.

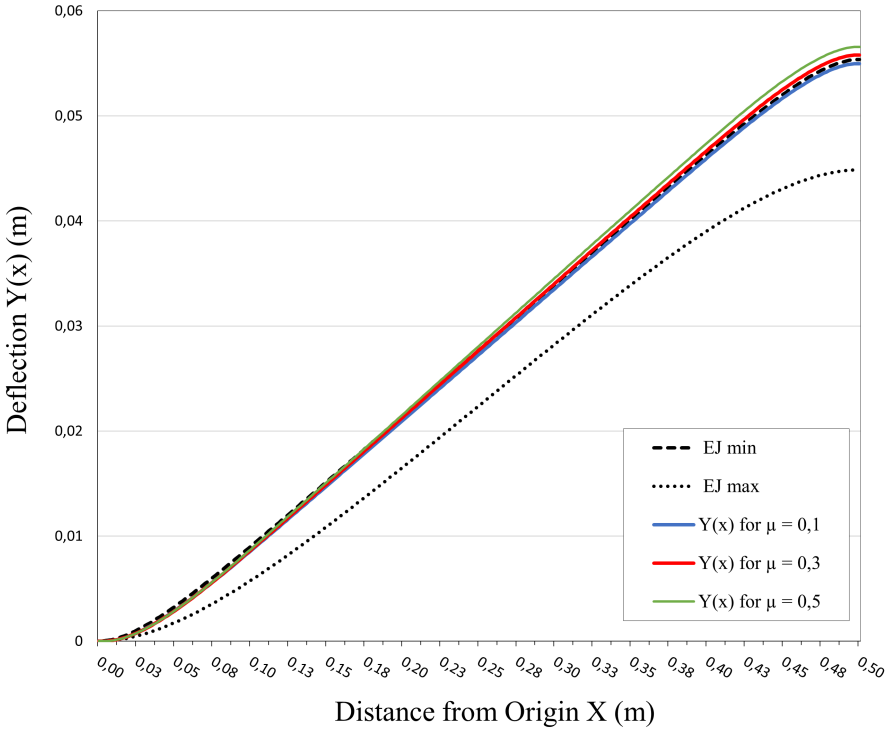


Figure 10. Deflection $Y(x)$ (m) from point $B$ (Origin) to the halfway mark (load $V$).

lines of $EJ_{min}$ and $EJ_{max}$, as these represent the extreme conditions for a conductor under bending, full slip and full stick-states, respectively. Not only all cases are very close or exceeding the minimum analytical bending stiffness, but Fig. 10 shows that the the model with the greater friction coefficient has the most total deflection, according to the literature, it should be the very opposite and no model should exceed the $EJ_{min}$ curve.

Table 5. Percentage difference for deflection $Y(x)$ $vs$ $EJ_{min}$

| **Friction Coef.** $\mu$ | **Deflection** $Y(x)$ **(mm)** | % **Diff** $EJ_{min}$ |
|---|---|---|
| $0,1$ | $54,96$ | $-0,74\%$ |
| $0,3$ | $55,79$ | $0,76\%$ |
| $0,5$ | $56,55$ | $2,14\%$ |
| **Average** | - | $0,72\%$ |

In order to further comprehend the model, Tab. 5 demonstrates that the numerical results have an average final deflection equivalent to the deflection obtained by $EJ_{min}$. These small divergences indicate a full slip state in all models, regardless of the variation in $\mu$. It is important to note that the region with maximum deflection $Y(x)$ is also the same in which the load V is applied. This region is subject to complex interactions and, in such non-linear problems, these small discrepancies do not interfere with the validity of the model.

Using the simulation with $\mu = 0,3$ as an example, Fig. 9 shows that there is a high magnitude of stress at deflection points in the conductor. Therefore, Fig. 11 is generated, which presents the deflection in the region near Support B, the origin of the model. This region is of great importance since it is a neutral region of the model, without restrictions from loads or boundary conditions, where only the interactions between the wires are in action.

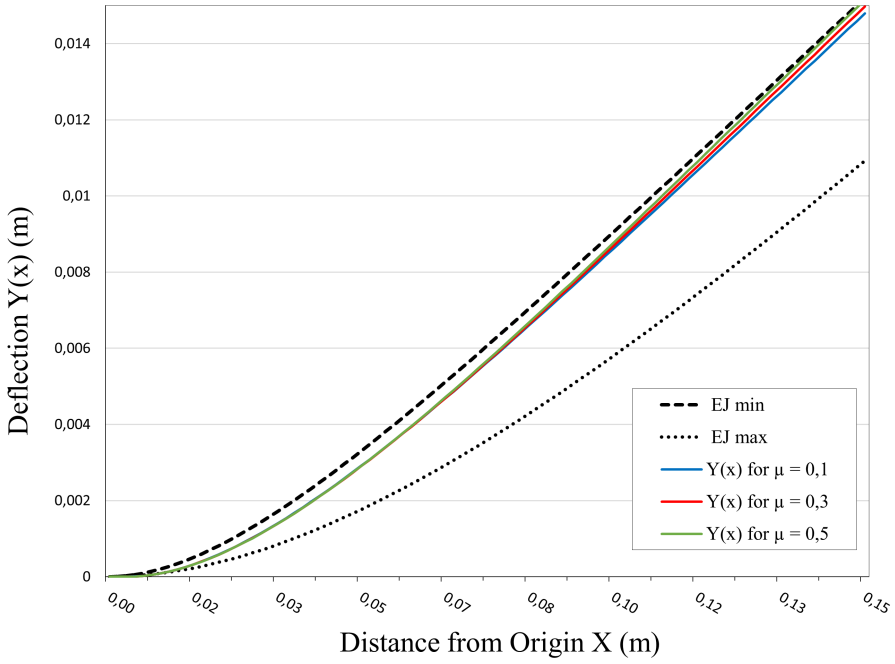


Figure 11. Deflection $Y(x)$ (m) near point $B$ (Origin).

In this region, a significant section rotation, curvature, is observed. Between 0 and 0,15 mm from the origin, there is a cable section where all three conductors deflect with the same magnitude and stiffness, as seen in Fig. 11. Furthermore, in this region, all evaluated conductors fall within the minimum and maximum lines, indicating results in line with the theory.

## 5. CONCLUSION

Based on the conducted studies, the parametric model developed in this work allows for the analysis of multilayered conductor cables with diverse geometric and physical properties. Changes between different cable configurations, materials, and boundary conditions showed low complexity and labor intensity in its execution, demonstrating the range and adaptability of the parametric model for conducting analyses.

The results for the tension simulations are within the expected range for the four cases analyzed. Furthermore, the axial displacement from the simulations is closer to analytical results than the corresponding values found by Wu (2014), as shown in Figure 8. The axial stresses in the layers also yield good results in general, with a maximum percentage difference of $21\%$ compared to analytical results and $31\%$ compared to those achieved by Wu (2014), as shown in Table 4.

The bending simulations also produces good results for the three cases studied. The deflection line as a function of the axial distance, as shown in Figure 11, falls within the maximum and minimum limits of the analytical formulation, indicating a region with the increase of bending stiffness expected from multilayered conductor's theory. The total deflection of the conductor is, on average, only $0,72\%$ higher than analytical results for the expected maximum deflection, as shown in Table 5. But the inverse deflection for ascending friction coefficients $\mu$ is a point that requires further testing to understand if there is a lack of proper friction response in the model and/or if the load $V$ application method is incompatible to the present model.

The objective of conducting simulations with low computational cost is also achieved, as confirmed by Table 3, which shows a reduction in consumed time of more than two orders of magnitude compared to solid element simulations. It can

be inferred that the present model is on par with the one presented by Lalonde *et al.* (2017).

In conclusion, the developed parametric model is satisfactory, but requires further testing, specially in bending simulations, aiming to numerically analyze multilayered conductor cables under bending and different friction coefficients.

## 6. REFERENCES

ANSYS APDL User's Guide, 2022. "Ansys apdl user's guide, 2022r2 15/12/22".

Cardou, A., 2013. *Stick-slip Mechanical Models for Overhead Electrical Conductors in Bending; with MatLab Applications*. Alain Cardou. ISBN 9782981233721.

Judge, R., Yang, Z., Jones, S. and Beattie, G., 2012. "Full 3d finite element modelling of spiral strand cables". *Construction and Building Materials*, Vol. 35, pp. 452 – 459. ISSN 0950-0618. doi:https://doi.org/10.1016/j.conbuildmat.2011.12.073. URL http://www.sciencedirect.com/science/article/pii/S095006181100763X.

Lalonde, S., Guilbault, R. and Légeron, F., 2017. "Modeling multilayered wire strands, a strategy based on 3d finite element beam-to-beam contacts - part i: Model formulation and validation". *International Journal of Mechanical Sciences*, Vol. 126, pp. 281 – 296. ISSN 0020-7403. doi:https://doi.org/10.1016/j.ijmecsci.2016.12.014. URL http://www.sciencedirect.com/science/article/pii/S0020740316305914.

MA, J., rong GE, S. and kun ZHANG, D., 2008. "Distribution of wire deformation within strands of wire ropes". *Journal of China University of Mining and Technology*, Vol. 18, No. 3, pp. 475 – 478. ISSN 1006-1266. doi:https://doi.org/10.1016/S1006-1266(08)60098-X. URL http://www.sciencedirect.com/science/article/pii/S100612660860098X.

Nawrocki, A. and Labrosse, M., 2000. "Finite element model for simple straight wire rope strands". *Computers Structures*, Vol. 77, pp. 345–359. doi:10.1016/S0045-7949(00)00026-2.

Papailiou, K.O., 1995. *Bending of helically twisted cables under variable bending stiffness due to internal friction, tensile force and cable curvature*. Ph.D. thesis, Eidgenössiche Technische Hochschule Zurich, Zürich, Switzerland. URL https://doi.org/10.3929/ethz-a-001442538.

Papailiou, K.O., 1997. "On the bending stiffness of transmission line conductors". *IEEE Transactions on Power Delivery*, Vol. 12, No. 4, pp. 1576–1588. doi:10.1109/61.634178.

Stanová, E., Fedorko, G., Fabian, M. and Kmet, S., 2011. "Computer modelling of wire strands and ropes part ii: Finite element-based applications". *Advances in Engineering Software*, Vol. 42, pp. 322–331. doi:10.1016/j.advengsoft.2011.02.010.

Wu, J.J., 2014. "The finite element modeling of spiral ropes". *International Journal of Coal Science Technology*, Vol. 1, pp. 346–355. doi:10.1007/s40789-014-0038-x.

## 7. RESPONSIBILITY NOTICE

The authors are solely responsible for the printed material included in this paper.